

Production of fast and slow particles in nucleus-nucleus collisions at ultrarelativistic energies

P. L. Jain, K. Sengupta, and G. Singh

High Energy Experimental Laboratory, Department of Physics, State University of New York at Buffalo, Buffalo, New York 14260

(Received 27 April 1990)

Multiplicity and angular distributions of shower, grey, and black particles produced in the interactions of ^{32}S at $200A$ GeV, ^{16}O at 200 and $60A$ GeV, and ^4He at $\sim 140A$ GeV in emulsion are compared with the predictions of a Monte Carlo code which takes into account the internuclear cascading. The correlations between the various parameters belonging to the same or to the different kinds of particles are discussed. The data on shower and grey particles from all the beams are well described by the code. However, the black prong data show a significant departure from this model.

I. INTRODUCTION

At ultrahigh energies, nuclear targets offer a unique opportunity to learn about the space-time development of the formation of secondary hadrons within very small distances and short times from the impact, which is definitely not possible in normal hadron-hadron interactions. A target nucleus serves as a detector of the products of the initial reaction. Naturally, the main problem is to find out what kind of signals these detectors send out.

In ultrarelativistic nuclear collisions the secondary hadrons are not formed instantaneously. There is a formation time between the interaction and the final hadronization of the particles. Due to time dilation, this time is long in the laboratory frame for fast particles, which undergo practically no rescattering in the nucleus, and is short for slow particles. They hadronize within the target and may reinteract with the surrounding target matter and produce cascade particles. The transition region between the two situations is very diffuse. This is partially due to the lack of exclusive experimental data in the target fragmentation region and partly due to the absence of good theoretical models which could take care of the production of the cascading particles. Theoretically, we do not have a good understanding of the space-time development of the evolution of particles in hadronic collisions. Little is known about the rate at which energy is deposited in the target nucleus. It depends on the number of nucleons with which the incident hadron interacts. Without the correct estimation of cascade interactions, which play a very important role, especially in the small pseudorapidity region, called the target fragmentation region, it will be dangerous to derive any conclusions about the new aspects from heavy-ion collision experiments. We know very little about how the observed final state of particles is related to the early stage of the interaction. We shall address these important issues in this paper.

Our objective is to employ the interactions of ^{16}O , ^{32}S , and ^4He in nuclear emulsion. The emulsion has the unique property of acting simultaneously as the target as

well as the detector, for registering all the charged particles in a 4π geometry with the highest spatial resolution (along the beam tracks) as compared to the electronic detectors. Thus, the angles of shower particles produced in ultrarelativistic nuclear interactions in the very forward direction are effectively measured with respect to the primary beam. The study of heavy-ion interactions in emulsion has another important advantage: one can study the low-energy short tracks of heavy fragments that are produced from the target fragmentations (TF's). But, when the TF's are very heavy and very short in length like small stems, it is rather hard to analyze them in emulsion. On the contrary, the tracks due to projectile fragmentations (PF's) in peripheral interactions are long and provide good pictures. These properties shall be utilized in the detection of PF's and TF's.

Section IV deals with the experimental results and is divided into two parts. In part A, we discuss the properties of the fast shower particles and in part B we discuss the general properties of the target-induced slow particles produced in the interactions of heavy-ions in emulsion. We shall discuss the cascading mechanism where the produced secondaries from the primary collisions reinteract with the surrounding target matter (target fragmentation region). The properties of these target induced particles are checked with the string model VENUS (version 3.05), which reproduces rather successfully the particle properties observed in this experiment. By comparing the experimental data with the string model (VENUS), we shall try to get some information about the interaction radius (r_0) of the VENUS model, which is essential for the interactions between nuclei.

II. THEORETICAL DISCUSSIONS

Recently, a great deal of interest has arisen in the study of ultrarelativistic nuclear collisions with the hope that one may produce the new form of matter known as the quark gluon plasma (QGP), which is the high-temperature and high-density phase of matter described

TABLE I. Details of the samples generated by VENUS (the symbols are explained in the text).

Beam	Energy (A GeV)	r_0 (fm)	σ (mb)	$\langle n_s \rangle$	$\langle N_b \rangle$	$\langle N_g \rangle$
^{32}S	200	0.5	1208	80.10	0.46	2.08
^{16}O	200	0.5	1039	57.77	0.49	1.97
^{16}O	60	0.9	1015	36.32	0.78	2.64
^4He	~ 140	0.5	748	27.37	0.48	1.83

by the laws of quantum chromodynamics. At low temperatures and densities, quarks, gluons, and color fields are confined to the interiors of the strongly interacting particles, thus there is a small chance to detect them. At high temperatures and densities, the hadrons overlap and lose their identity. Quarks, gluons, and color fields are not confined within hadrons, but can move over distances larger than the hadron size, 1 fm.

Experimentally, we have learned that geometrical effects play an important role in nucleus-nucleus collisions. In a majority of collisions, only a part of the incident nucleus interacts. For the formation of the QGP, one has to trigger on those events in which the entire beam nucleus interacts. Under the present experimental conditions, a mixed phase appears to dominate the important phenomenon and this creates additional complications. Thus, at present the situation is rather confusing. Theoretical estimations suggest that the energy densities achieved are sufficient to produce the plasma. Perhaps the plasma has already been produced in ultrarelativistic nucleus-nucleus collisions; however, it has not yet been unambiguously identified.

In building theoretical models, the theoreticians have used the basic models for hadron-nucleus collisions and have extended them to nucleus-nucleus collisions: the common models are the multichain model [1], the additive quark model [2], the dual parton model or the cascade model [3,4]. Some of these models do not have rescattering of the secondaries built into their formalisms, with the result that the experimental data do not match with theoretical predictions in that η range. Recently, two models, multichain fragmentation model (MCFM) [5], and VENUS [6], based on the dual fragmentation scheme of Capella *et al.* [3], at least partially take cascading into account. In the MCFM, cascading is introduced artificially by treating an empirical parameter τ_0 , related to the hadronic formation time, as a free parameter. In the VENUS model (version 3.05), rescattering is determined by the *interaction radius* r_0 . This means that

whenever two particles come closer than r_0 , they interact. A comparison with the experimental data on target related particles should reveal the magnitudes of these parameters. The interaction radius r_0 is an important quantity as it plays an important part in determining the energy density and hence in the formation of QGP. In this paper, we shall test the cascade model VENUS for a number of physical properties of the fast and slow produced particles, some for the first time in ultrarelativistic nucleus-nucleus collisions.

We used VENUS to generate reference samples of 1000 minimum-bias events corresponding to interactions of each of the ^{32}S at 200 A GeV (beam A), ^{16}O at 200 A GeV (beam B) and ^{16}O at 60 A GeV (beam C) and stored the stable charged particles only. The fraction of the events from the different target nuclei in emulsion was generated using the known chemical composition of the emulsion as an input to the model. The inelastic cross sections (σ) of the simulated events are in good agreement with the data, as shown in Tables I and II. Classification of particles according to the emulsion terminology is discussed in the following section.

III. EXPERIMENTAL PROCEDURE

Emulsion stacks of the EMU08 experiment were exposed horizontally to ^{32}S (beam A) and ^{16}O (beam B) ions at 200 A GeV and ^{16}O (beam C) ions at 60 A GeV at the CERN SPS. Details of the experimental procedure can be found in Ref. 7. The primary interactions were found by along-the-track scanning of the emulsion plates. The samples of events thus obtained, for each of the projectiles A, B, and C, are bias free and will be referred to as the *minimum-bias* events. (The minimum ionizing shower tracks include the spectator protons from the projectile.) From these samples, we have excluded the electromagnetic [9] and elastic scattering events.

In emulsion experiments, the velocity (ionization) determination leads conventionally to the following groups of particles.

N_b : the number of *black* particles having velocity $\beta = v/c \leq 0.2$. These are the fragments of the target nucleus. For a proton track, the kinetic energy is < 20 MeV.

N_g : the number of *grey* particles with velocity $0.2 \leq \beta \leq 0.7$. They are often assumed to be protons with kinetic energy $20 < E_k < 400$ MeV. At high energies, the average number $\langle N_g \rangle$ depends little on energy, and its increase with the mass A can be derived from a universal dependence on the average number of inelastic collisions

TABLE II. The experimental average multiplicities of shower, black, and grey particles.

Beam	Energy (A GeV)	σ (mb)	$\langle n_s \rangle$	$\langle N_b \rangle$	$\langle N_g \rangle$
^{32}S	200	1140 ± 36	79.20 ± 4.1	4.97 ± 0.26	2.25 ± 0.12
^{16}O	200	1101 ± 60	57.30 ± 3.1	5.39 ± 0.29	2.03 ± 0.11
^{16}O	60	990 ± 44	34.12 ± 2.3	4.91 ± 0.34	2.16 ± 0.15
^4He	~ 140	602 ± 30	23.59 ± 1.2	5.44 ± 0.27	1.66 ± 0.08

$\langle \nu \rangle$. To obtain an event-by-event estimate we define $\langle \nu \rangle = c\sqrt{N_g}$ [8], where c is a constant. We may point out that not all the recoil nucleons end as grey or black tracks; nucleons with much higher momenta are also produced.

N_h : the number of heavy particles defined as $N_h = N_g + N_b$ and $\beta \leq 0.7$.

n_s : the number of shower particles. These are assumed to be mostly produced pions having $\beta > 0.7$.

A comprehensive discussion of the classification and identification of the events in emulsions can be found in Ref. [9]. The polar angles (θ_i) of the tracks were determined from the vector directions of the emitted tracks with respect to a noninteracting beam track (the reference primary track) selected in the vicinity of the interaction vertex. The xyz coordinates of all the tracks, including the vertex and the reference primary track were subjected to least-squares, three-dimensional track reconstruction programs which gave the polar angles. This technique gives an accuracy better than 0.1 mrad for angles $\theta \leq 1$ mrad, including the error due to multiple Coulomb scattering.

Although the yield of target-related heavy fragments does not change dramatically when one employs heavy-ion projectiles in place of the proton beam, instead the use of heavy-ion beams introduces an important experimental advantage over the proton beam. One can study the relativistic heavy projectile fragments which are produced by the disintegration of the ultrarelativistic projectile nucleus. Previously [9], we have studied the disintegration of ${}^4\text{He}$ fragments in ${}^{32}\text{S}$ at 200 A GeV and also from ${}^{16}\text{O}$ beams at 200 and 60 A GeV [10] in emulsion. The production cross sections for 1 He ($\sigma_{1\alpha}$), 2He ($\sigma_{2\alpha}$), 3He ($\sigma_{3\alpha}$), and 4He ($\sigma_{4\alpha}$) were determined to be 306 ± 19 , 147 ± 13 , 64 ± 9 , and 18 ± 5 mb, respectively. Since there is no low-mass ion (lighter than the mass of ${}^{16}\text{O}$) like He available from accelerators with energy $> 100 A$ GeV, no data exist on the secondary inelastic interactions of a He beam with stationary targets at such energies. We therefore have collected all the He fragments disintegrated from the ${}^{32}\text{S}$ beam at 200 A GeV in nuclear emulsion [11]. A total of 1354 events of the ${}^{32}\text{S}$ nucleus was picked up by following 127.38 m of the primary track length. Out of 1354 events, 1157 events were due to inelastic interactions. Among the 1157 inelastic events, 923 events were found to be peripheral [7,9]. The He fragments produced from parent stars of ${}^{32}\text{S}$ in emulsion were identified by counting the grain density or gap density as discussed in Refs. [7,9,10]. A total of 1110 He tracks was selected in 640 inelastic (peripheral) events. Theoretically, He being a projectile fragment of ${}^{32}\text{S}$ (beam A) should have the same energy per nucleon as that of the parent beam, but as they are produced from peripheral interactions, there is some loss of energy for these fragments, which varies from event to event. The average energy of He fragments varies in the range of 130–170 A GeV. There is no direct way of measuring their average energy; however we can estimate it by indirect means as described in Sec. IV A 1. It is reasonable to treat the projectile He fragments just like another new primary ultrarelativistic

beam. This is the advantage of using nuclear emulsion as a detector in the field of heavy ion physics.

By following 104.55 m of the track length of He tracks (beam D), 497 secondary inelastic interactions were recorded. The details of this experiment are given in Refs. [7,9,10]. The grey and black tracks were recorded for each event and the angles of shower, grey, and black tracks were measured as discussed before.

IV. RESULTS

A. Shower particles

1. Shower-particle multiplicity

For minimum-bias events the average shower-particle multiplicities $\langle n_s \rangle$ corresponding to beams A–D seem to vary with the total kinetic energy of the projectile E_T according to the relation $\langle n \rangle = aE_T^b$, where $a = 32.72$ and $b = 0.47$, and are shown in Fig. 1(a). From this universal curve, corresponding to the average multiplicity of $\langle n_s \rangle = 23.6 \pm 1.2$, the energy of the ${}^4\text{He}$ beam D per nucleon $\approx 140 A$ GeV. The dispersion (D) of the multiplicity distributions corresponding to all the projectiles is

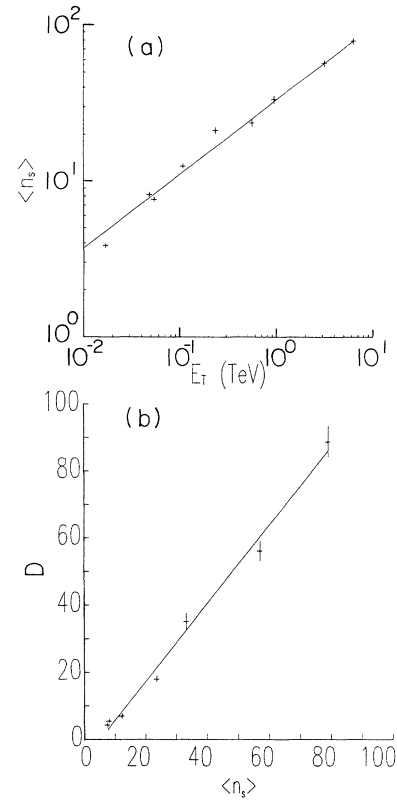


FIG. 1. (a) $\langle n_s \rangle$ as a function of the total kinetic energy E_T of the projectile. The solid line represents a power-law fit to the data (see text). (b) D vs $\langle n_s \rangle$. The solid line is a least-squares fit to the data. The low-energy data in these figures are taken from Refs. [15–17].

given by the relation $D = a + b \langle n_s \rangle$, where $a = -6.01 \pm 1.92$ and $b = 1.16 \pm 0.05$, and is shown in Fig. 1(b).

The multiplicity distributions of the shower particles produced in the minimum-bias events of beams A–D are shown in Figs. 2(a)–2(d), respectively. The broken histograms in Figs. 2 represent the predictions of VENUS, which are in good agreement with the experimental data for the projectiles A–C. As the energy for each of the He fragments was not the same, we did not try to match the experimental data with the predictions of VENUS at any value of beam energy. The maxima of the data as well as of the model predictions are towards the low values of multiplicities and are highest for the lowest projectile energy (viz. ^{16}O at 60 A GeV). In the cases of beams A–C, the heights of the maxima fall off characteristically with energy, while the tail extends with energy. The experimental values of $\langle n_s \rangle$ for projectiles A–D are given in Table II. A comparison with Table I shows that $\langle n_s \rangle$ is

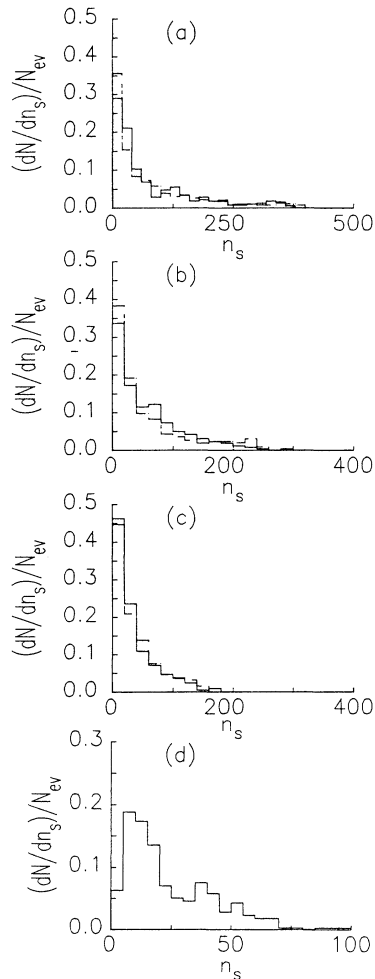


FIG. 2. The normalized shower-particle multiplicity distributions for (a) 200 A GeV ^{32}S , (b) 200 A GeV ^{16}O , (c) 60 A GeV ^{16}O , and (d) ~ 140 A GeV ^4He . The broken histograms are the corresponding predictions of VENUS.

reproduced quite well by the model in each of the projectiles.

In Fig. 3, we show the multiplicity distribution for beams A–D when expressed in the normalized form $\langle n_s \rangle \sigma_n / \sigma_{\text{inel}}$ as a function of the scaled variable $n_s / \langle n_s \rangle$. The distribution exhibits a universal scaling within the statistical errors irrespective of the projectile mass and energy. The theoretical prediction of VENUS for beam B is shown in Fig. 3, where the agreement with the data is quite good. The behaviors of other beams are exactly the same. The origin of the multiplicity scaling is a consequence of the nuclear geometry (impact parameter). For the ^{32}S beam, there is a small bump at high values of $n_s / \langle n_s \rangle$, which is due to the fact that the collision, with a relatively broad range of the central impact parameters, involves a nearly constant number of participants.

2. Pseudorapidity

One of the fundamental experimental distributions in high-energy collisions that is generally compared with any successful theoretical model is the pseudorapidity ($\eta = -\ln \tan \theta/2$) distribution of the produced shower particles. In Figs. 4(a)–4(c) we compare the pseudorapidity distributions of the shower particles from the interactions of projectiles A–C, respectively, in emulsion, with the corresponding predictions of VENUS. The experimental pseudorapidity distributions in each case are in good agreement with the model for the values of r_0 indicated in Table I except in the very forward region, where the disagreement is due to the noninclusion of spectator particles in the model. The heights and widths of the distributions increase with the increase in the energy and mass of the projectile. As the He fragments are not monoenergetic, it is difficult to assign one specific input value in the theoretical model to generate secondary par-

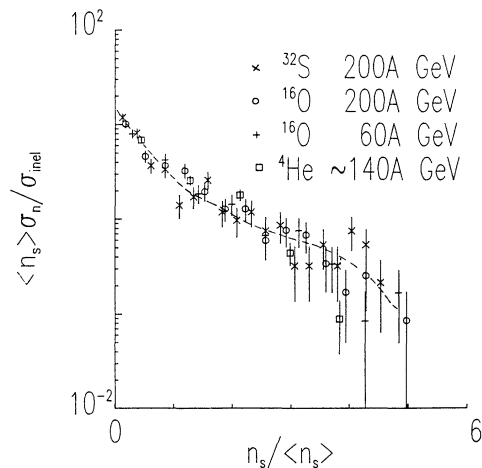


FIG. 3. $\langle n_s \rangle \sigma_n / \sigma_{\text{inel}}$ as a function of $n_s / \langle n_s \rangle$: 200 A GeV ^{32}S (x), 200 A GeV ^{16}O (o), 60 A GeV ^{16}O (+), and ~ 140 A GeV ^4He (□). The dotted curve is the theoretical prediction for beam B.

ticles to match with the experimental data. In Fig. 4(d) is shown the pseudorapidity distributions (η) for the four beams A–D together. The η distributions of beams A, B, and C scale in the target fragmentation region for $\eta \leq 1.8$. This is due to the range of impact parameters in terms of geometrical models. For beams A, B, and D, the centers of the η distributions lie very close together near $\eta \approx 3.4$, while for beam C (^{16}O at 60 A GeV) the center is shifted towards low value, i.e., $\eta \approx 2.4$. Thus, the experimental η distribution of beam D indicates that the energy per nucleon of the He beam D is of the same order of magnitude as those of beams A and B and definitely greater than 100 A GeV.

Having tested the VENUS model in Figs. 2 and 4, we now turn to the distributions of the slow particles (viz.

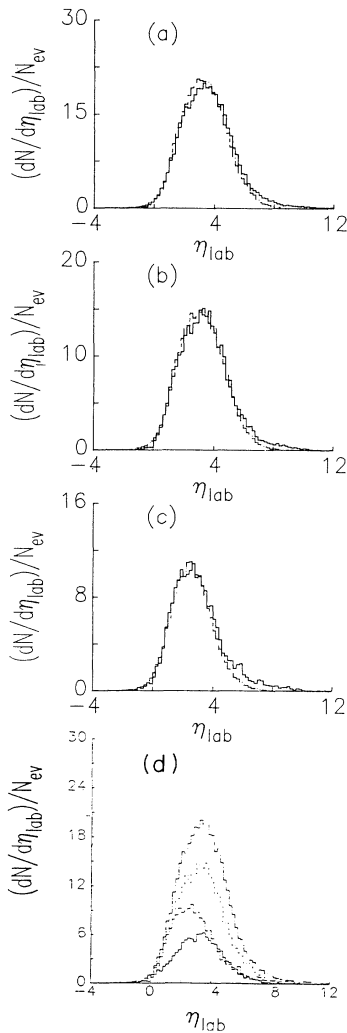


FIG. 4. The normalized pseudorapidity distributions at (a) 200 A GeV ^{32}S , (b) 200 A GeV ^{16}O , (c) 60 A GeV ^{16}O . (d) A comparison of the pseudorapidity distributions of the above three beams and that of the ^4He projectile at ~ 140 GeV/nucleon. The broken histograms are the corresponding predictions of VENUS.

black and grey), as defined in Sec. III. Table II shows the summary of the multiplicities of black, grey, and shower particles for interactions of the four projectiles in emulsion. The data show that within experimental uncertainties, the average multiplicities $\langle N_g \rangle$ and $\langle N_b \rangle$ do not depend on the incident energy and mass of the projectiles considered at such high energies. The energy and mass independence of the projectiles in the production of the slow particles at such high-energy heavy-ion interactions reflect the limiting behavior of the nuclear fragmentation process. The energy independence of $\langle N_g \rangle$ and $\langle N_b \rangle$ has been observed earlier in hadron-nucleus collisions [12], although its mechanism was not well understood. An extension of the limiting fragmentation process (in terms of energy and mass of the projectile) for slow particles in heavy-ion collisions is valid, but it poses the even more formidable challenge of understanding the underlying mechanism. The values of the interaction radius r_0 which reproduce $\langle N_g \rangle$ values very close to beams A–D through VENUS are 0.5, 0.5, 0.9, and 0.5 fm (see Table I), respectively. However, for the same r_0 values $\langle N_b \rangle$ is strikingly underestimated for all the beams A–D. The lack of agreement of black-particle distributions in VENUS and the data suggest that the model does not have an adequate cascading in the target.

3. Shower- and grey-particle correlations

Previous work on nuclear interactions in emulsion has shown that the number of grey tracks emitted from an in-

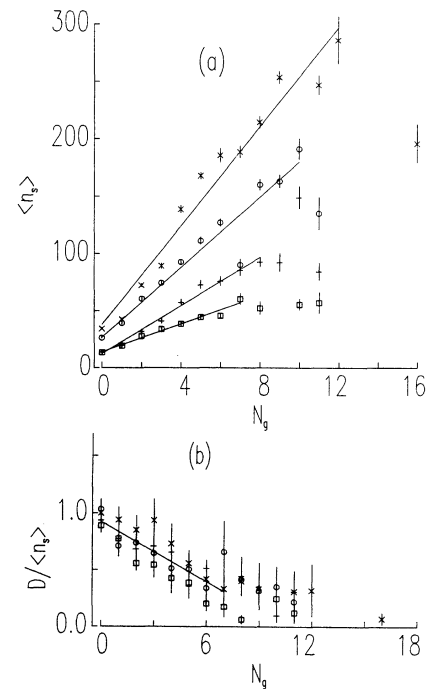


FIG. 5. (a) The correlation between $\langle n_s \rangle$ and N_g . The solid lines are least-squares fits to the data corresponding to each projectile (see text). (b) $D/\langle n_s \rangle$ as a function of N_g . The straight line represents a least-squares fitting to the data (see text). The symbols used here are as in Fig. 3.

TABLE III. The coefficients a_i and b_i in $\langle n_s \rangle = a_i + b_i N_g$ (see text).

Beam	Energy (A GeV)	a_i	b_i	χ^2/DOF
^{32}S	200	38.09 ± 9.14	21.53 ± 1.35	2.20
^{16}O	200	26.88 ± 9.09	15.30 ± 1.54	2.70
^{16}O	60	12.48 ± 2.40	10.53 ± 0.50	0.29
^4He	~ 140	14.18 ± 1.74	6.12 ± 0.42	0.16

teraction is related to the number of inter-nuclear collisions experienced by the projectile [8]. We extend this idea to nucleus-nucleus collisions. The mean multiplicities $\langle n_s \rangle$ are plotted against the number of grey tracks (N_g) for the four beams in Fig. 5(a). The data corresponding to each beam show a linear relation between $\langle n_s \rangle$ and N_g and support the important assumption that there is a positive correlation between the average number of target fragments and the mean number of inter-nuclear collisions (ν). The correlation between $\langle n_s \rangle$ and N_g is given by $\langle n_s \rangle = a_i + b_i N_g$, where the fitted values of the coefficients a_i and b_i are given for all the four beams in Table III.

In Fig. 5(b), we show $D/\langle n_s \rangle$ as a function of N_g corresponding to all the four projectiles. The distribution is expressed by the relation $D/\langle n_s \rangle = c_1 + d_1 N_g$, where $c_1 = 0.93$ and $d_1 = -0.09$ with $\chi^2/(\text{DOF}) = 0.03$ (DOF denotes degrees of freedom). The fitting is done up to $N_g \approx 6$ for statistical reason. This distribution is almost independent of the projectile energy and mass for the same target.

The pseudorapidity distributions of shower particles produced in nucleus-nucleus collisions were shown earlier in Figs. 4. Now we present the characteristics of $\langle \eta \rangle$ as functions of N_g for beams A–D in Fig. 6, where the data points have been fitted with polynomials. We notice that all curves slowly decrease due to the loss of the projectile energy with increasing number of collisions (large N_g)

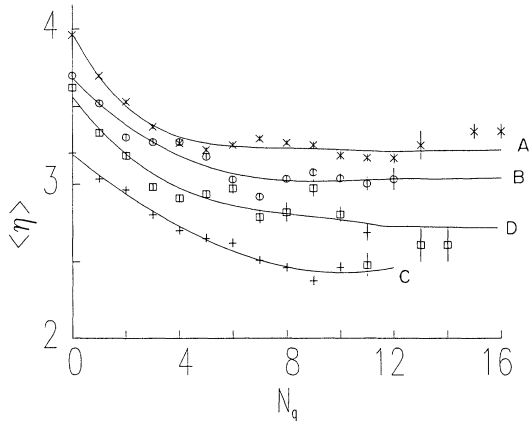


FIG. 6. $\langle \eta \rangle$ as a function N_g . The curves represent polynomial fits to the data. For the equation of the solid curve, see text. The symbols are described in the caption of Fig. 3.

and eventually level off. The energy is shared by more and more particles at less and less energy.

4. Comparisons of grey-particle production with VENUS

In Figs. 7(a)–7(d), the N_g distributions of the four data samples are compared with reference samples generated by VENUS. The agreement is very good for the values of r_0 indicated in Table I. The experimental data extend to higher N_g values for beam A as compared to beams B

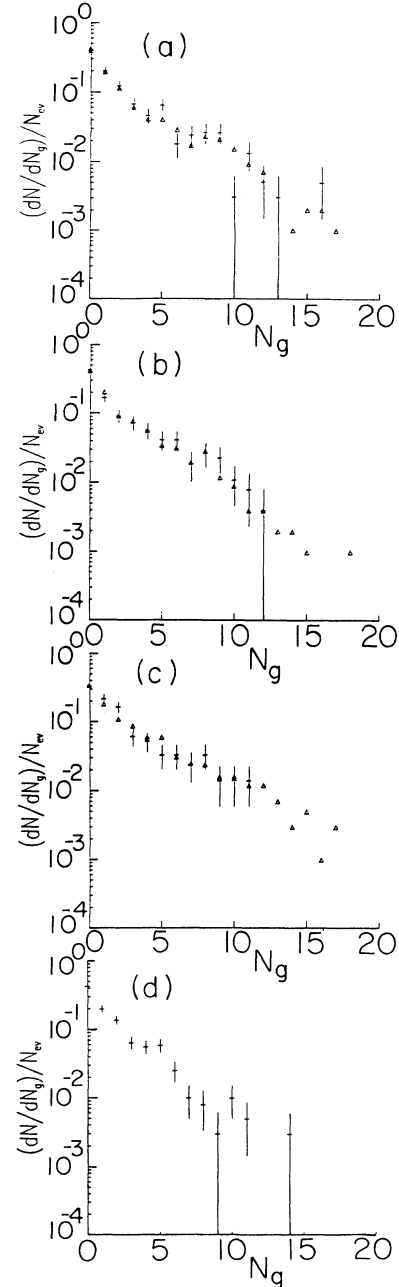


FIG. 7. The normalized multiplicity distributions of grey prongs at (a) 200 A GeV ^{32}S , (b) 200 A GeV ^{16}O , (c) 60 A GeV ^{16}O , and (d) ~ 140 A GeV ^4He . The corresponding VENUS predictions (Δ) are shown in (a), (b), and (c).

and C. In Fig. 8, we show the N_g distributions corresponding to the four projectiles A–D together. The data overlap up to $N_g \approx 6$, where the statistics is reasonably good for all the beams. The grey-particle distribution seems to be independent of incident energy as well as the projectile mass within statistical errors up to $N_g \approx 6$.

5. Angular distributions of grey particles

Figures 9(a)–9(d) deal with the angular distributions of grey particles for projectiles A–D, respectively, along with the corresponding predictions from VENUS. We find that the spectra generated by the model are slightly forward peaked compared to the data in each case. The overall fitting for beam C is better than in beams A and B. The angular distributions of grey particles produced from interactions of projectiles A–D in emulsion are distinctly anisotropic. In general, multiplicity and angular distributions of grey particles have been reproduced very well by the theoretical model VENUS, except in the region of $\cos\theta < -0.3$ for the angular distributions. In Figs. 10(a)–10(d) we show $\langle \cos\theta_j \rangle$ as a function of N_j (grey particles) for all the four beams and within the statistical errors they have the same shape, where j stands for the number of grey particles.

B. Grey and black particles

1. Angular distributions of black prongs

In Figs. 10(a)–10(d) we show $\langle \cos\theta_j \rangle$ as a function of N_j (j is for black particles) for all the four beams A–D. The distributions are flat for all N_j and extend up to $N_j \approx 20$. The angular distributions of black prongs when plotted in the normalized form $dN_b/d(\cos\theta_b)$ as a function of $\cos\theta_b$, exhibit near-isotropic distribution for all the four projectiles.

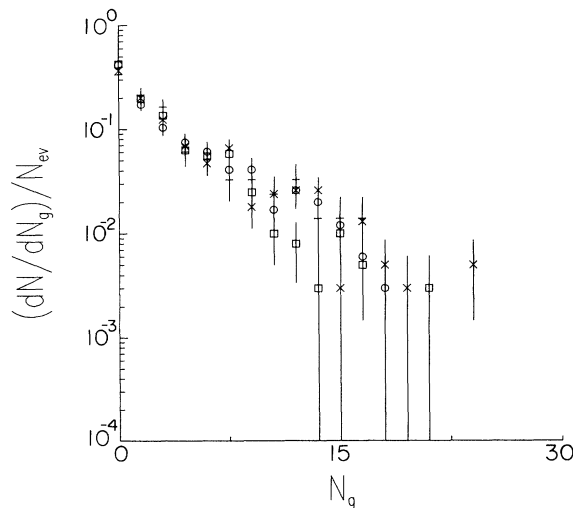


FIG. 8. A comparison of the grey prong multiplicity distribution corresponding to the four projectiles. See caption of Fig. 3 for a description of symbols.

2. Correlation between heavy particles

The integral frequency distributions of heavy tracks ($N_h = N_b + N_g$) are shown in Fig. 11(a), which are almost independent of the energy and mass of the projectiles. The curves have two different slopes with breaks approximately corresponding to the light (C, N, O) and heavy (Ag, Br) constituents of the emulsion target. The correlation between $\langle N_b \rangle$ and N_g is shown in Fig. 11(b), which can be expressed as a linear relation, i.e., $\langle N_b \rangle = c_2 + d_2 N_g$, where the coefficients $c_2 = 2.19$, $d_2 = 1.78$ with $\chi^2/\text{DOF} = 0.29$. The dependence of $\langle N_b \rangle$ increases with N_g up to ~ 6 , where the data have good statistics. The behavior exhibited is the same for all the four beams.

We now compare the N_b multiplicity distribution of

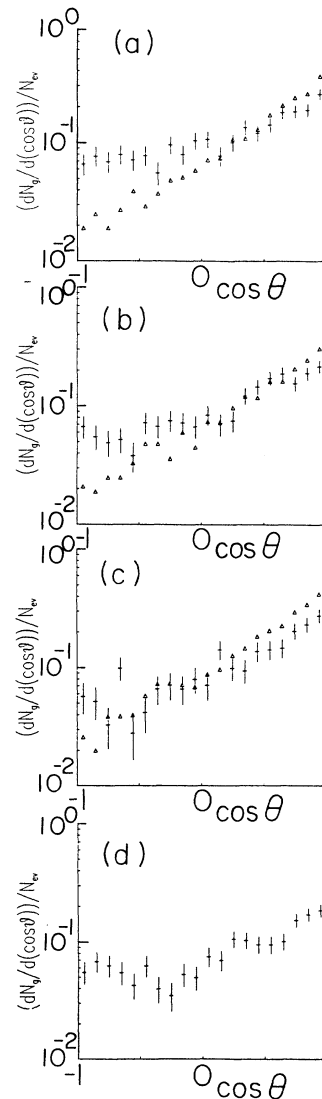


FIG. 9. The normalized angular distributions of grey prongs at (a) 200 A GeV ^{32}S , (b) 200 A GeV ^{16}O , (c) 60 A GeV ^{16}O , and (d) ~ 140 A GeV ^4He . The corresponding VENUS predictions (Δ) are shown in (a), (b), and (c).

the three data samples with the reference samples (beams A, B, and C) generated by VENUS for the same set of values of r_0 used in the context of the N_g distributions. These are shown in Fig. 12(a) corresponding to projectiles A and B (together) at 200 *A* GeV and in Fig. 12(b) for projectile C at 60 *A* GeV. The N_b distributions obtained from VENUS show a significant departure from the data. The combined experimental N_b distributions corresponding to the four beams A–D exhibit a behavior similar to that shown in Fig. 12(c).

The above observations therefore confirm the earlier conviction that grey particles are indeed remnants of reinteractions among the produced secondaries [1]. However, the simple rescattering mechanism included in VENUS is inadequate for explaining the distribution of the black particles, which are evaporation fragments of the target nucleus. The pseudorapidity distributions of the shower particles for projectiles A–C are in agreement with those of the VENUS predictions in the target fragmentation region. The observation that VENUS produces predominantly more protons in the grey-particle category testifies to the fact that the meson production in this region is hardly influenced by rescattering, while the baryon production is enhanced in the target fragmentation region. It is interesting to note that our results for the 200 *A* GeV ^{16}O data are in agreement with those of Ref. [12], where a different version of the dual parton

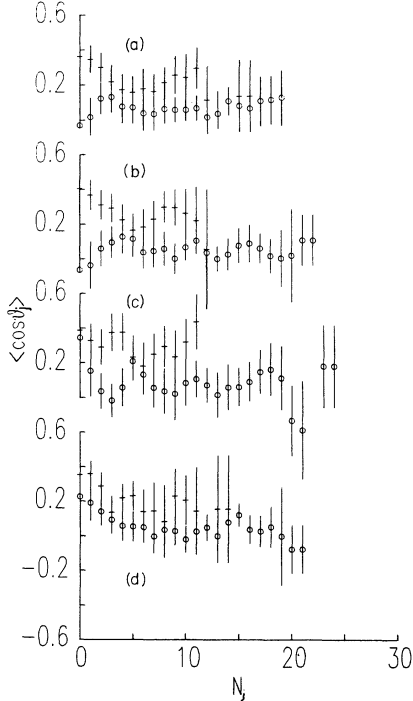


FIG. 10. The correlations between $\langle \cos\theta_j \rangle$ and N_j , where j stands for grey or black prongs: (a) 200 *A* GeV ^{32}S , (b) 200 *A* GeV ^{16}O , (c), 60 *A* GeV ^{16}O , and (d) ~ 140 *A* GeV ^4He . The distributions corresponding to grey prongs are shown by the symbol (+), and those corresponding to black prongs by (o). Here we include the points for $N_g=0$ or $N_b=0$.

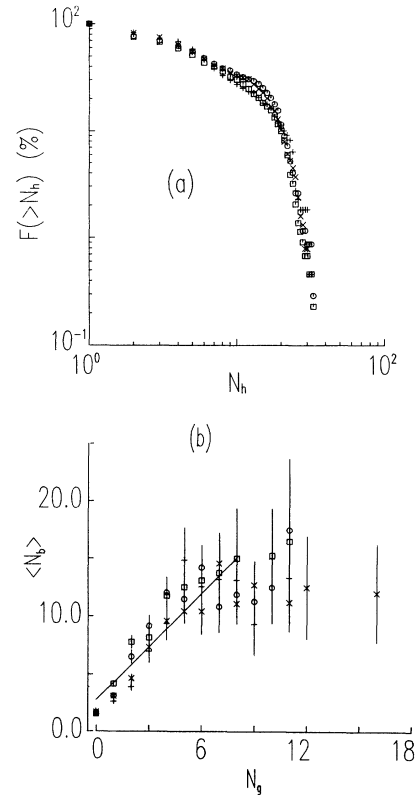


FIG. 11. (a) The integral N_h distributions and (b) the correlation between $\langle N_b \rangle$ and N_g . For the equation of a straight line in this figure, see text. The symbols are described in the caption of Fig. 3.

model, viz. MCFM, was used. It was concluded that MCFM can reasonably well explain the multiplicity spectra of grey particles when the free parameter τ_0 is set equal to 5 fm/c, while the evaporation process has to be treated in a more consistent manner to explain the multiplicity spectra of the black particles. Although the two approaches produce basically the same conclusions, it is worth noting that the concept of formation time seems somewhat artificial in the context of string models, where the formation point in space and time is given from the string dynamics. Also, assuming a single value of τ_0 is an oversimplification [13,14].

V. CONCLUSIONS

In the present paper we have studied the multiplicity and angular distributions of all the particles produced from the interactions of four different projectiles, viz. ^{32}S at 200 *A* GeV, ^{16}O at 200 and 60 *A* GeV, and ^4He at ~ 140 *A* GeV in nuclear emulsion.

For minimum-bias events, we have observed the following: for shower particles, the average multiplicity in emulsion is given by the power law $\langle n_s \rangle = aE_T^b$, where $a=32.72$ and $b=0.47$ and E_T is the total kinetic energy of the projectile nucleus. In our opinion, E_T is a good pa-

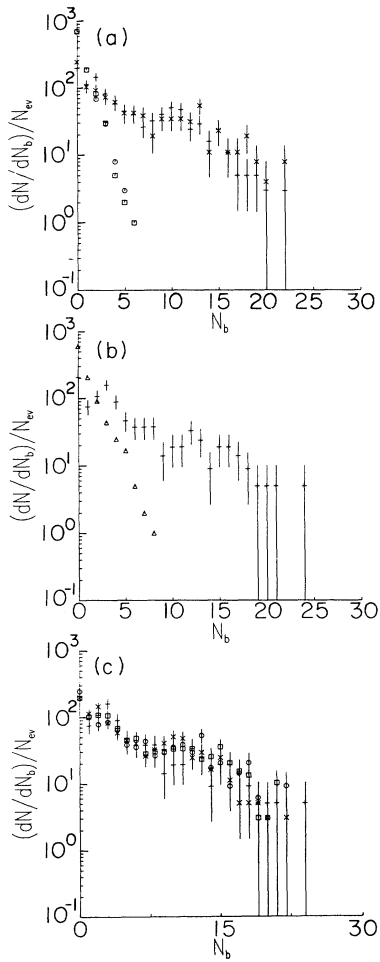


FIG. 12. The normalized multiplicity distributions of black prongs for (a) 200 A GeV ^{32}S and ^{16}O and (b) 60 A GeV ^{16}O . The corresponding VENUS predictions ($\circ, \square, \triangle$) are shown in each diagram. (c) A comparison of the angular distributions of black prongs corresponding to the four projectiles. The symbols are the same as those of Fig. 3.

parameter which determines the various thresholds and should be more often used. The dispersions of the multiplicity distributions can be given by a linear relationship in an analogy to the hadron-nucleon interactions:

$D = a + b \langle n_s \rangle$, where the values of the constants are $a = -6.01 \pm 1.92$ and $b = 1.16 \pm 0.05$.

The multiplicity and the angular distributions of the shower particles are well described by the predictions of the Monte Carlo code VENUS, which takes cascading into account. The multiplicity of the shower particles when plotted in the form $\langle n_s \rangle \sigma_n / \sigma_{\text{inel}}$ as a function of $n_s / \langle n_s \rangle$, shows almost a universal scaling. The center of the η distribution of the shower particles produced by the He beam (D) lies very close to the centers for beams A and B and is far away from beam C. This indicates that the energy per nucleon of beam D is approximately equal to that of beams A and B and is $\sim 200 A$ GeV.

Multiplicity correlations between the shower and grey particles for heavy-ion beams are given by the linear relation $\langle n_s \rangle = a + b N_g$. The coefficients grow with the projectile mass and energy. The distribution $D / \langle n_s \rangle$ decreases linearly with the increase in N_g , which indicates that the multiplicity distribution narrows towards lower η values as the number of interactions that the incident state experiences increases. The distribution of $\langle \eta \rangle$ with N_g decreases due to the loss of the projectile energy with increasing number of collisions or with collision of projectiles with more mass. Multiplicity and angular distributions of N_g particles are well described by VENUS, while for the same distributions of N_b particles the model predictions show a significant departure from the data. The correlation between $\langle N_b \rangle$ and N_g is given by a linear relation $\langle N_b \rangle = c_2 + d_2 N_g$, where the values of the coefficients c_2 and d_2 are given in Sec. IV B 2.

The new beam of ^4He projectile fragments produced from the soft interactions of ^{32}S ions (parent beam A) is used here for the first time. It has reproduced results compatible to its parent beam A as well as to the other beam B having the same energy per nucleon. We hope that this technique of obtaining a lighter-mass ion beam such as He from a heavier-mass projectile (^{32}S) will be used quite frequently in future experiments.

ACKNOWLEDGMENTS

We are thankful to the technical staff and the emulsion operating group of CERN for their help in the exposure, and to Professor G. Romano for his help in the development of our emulsion stacks. This work was supported by the Department of Energy under Grant No. DE-FG02-90ER40566.

- [1] K. Kinoshita, A. Minaka, and H. Sumiyoshi, *Z. Phys. C* **8**, 205 (1981).
- [2] A. Bialas, W. Czyz, and L. Lesniak, *Phys. Rev. D* **25**, 2328 (1982).
- [3] A. Capella, C. Pajares, and A. V. Ramello, *Nucl. Phys. B* **241**, 75 (1984); A. Capella and J. Tran Than Van, *Z. Phys. C* **10**, 249 (1981).
- [4] I. Otterlund, S. Garpman, I. Lund, and E. Stenlund, *Z. Phys. C* **20**, 281 (1983).
- [5] J. Ranft, *Phys. Rev. D* **37**, 1842 (1988); *Z. Phys. C* **43**, 439

- (1989).
- [6] K. Werner, *Phys. Lett. B* **208**, 520 (1988); *Phys. Rev. D* **39**, 780 (1989); K. Werner, CERN Report No. CERN-TH-5538/89, 1989.
- [7] P. L. Jain, K. Sengupta, G. Singh, and A. Z. M. Ismail, *Phys. Lett. B* **235**, 351 (1990); K. Sengupta, G. Singh, and P. L. Jain, *Mod. Phys. Lett. A* **5**, 285 (1990); *Phys. Lett. B* **236**, 219 (1990).
- [8] M. K. Hegab and J. Hufner, *Phys. Lett.* **105B**, 103 (1981); *Nucl. Phys. A* **384**, 353 (1982); W. Q. Chao, M. K. Hegab,

- and J. Hufner, *ibid.* **A395**, 482 (1983); B. Anderson, I. Otterlund, and E. Stenlund, *Phys. Lett.* **73B**, 343 (1978); P. L. Jain, K. Sengupta, and G. Singh, *Nuovo Cimento* **A99**, 9 (1988).
- [9] G. Singh, K. Sengupta, and P. L. Jain, *Phys. Rev. C* **41**, 999 (1990).
- [10] K. Sengupta, G. Singh, and P. L. Jain, *Phys. Lett. B* **222**, 301 (1989); G. Singh, K. Sengupta, and P. L. Jain, *Phys. Rev. C* **42**, 1757 (1990); K. Sengupta, G. Singh, T. Ritter, and P. L. Jain, *Europhys. Lett.* **8**, 15 (1989).
- [11] There are other He isotopes (^3He and ^6He) present in some proportion among the majority of ^4He projectile fragments, but these isotopes do not differ greatly in geometrical sizes in nuclear reactions at CERN energies.
- [12] P. L. Jain *et al.*, *Nucl. Phys.* **67**, 641 (1965); A. Abduzhamilov *et al.*, *Z. Phys. C* **40**, 223 (1988).
- [13] M. I. Adamovich *et al.*, *Phys. Lett. B* **234**, 180 (1990); M. I. Adamovich, *ibid.* **230**, 175 (1989).
- [14] L. Van Hove, CERN Report No. CERN-TH 5489, 1989.
- [15] V. S. Shukla *et al.*, *Mod. Phys. Lett. A* **3**, 1753 (1988).
- [16] Dipak Ghosh *et al.*, *Nucl. Phys.* **A499**, 850 (1989).
- [17] M. I. Adamovich *et al.*, *Phys. Rev. Lett.* **62**, 2801 (1989).